



## Measurement of the polarization of the $\Xi^0$ ( $\overline{\Xi^0}$ ) hyperon beam by the NA48/1 experiment

NA48/1 Collaboration

J.R. Batley, G.E. Kalmus<sup>1</sup>, C. Lazzeroni<sup>2</sup>, D.J. Munday, M. Patel<sup>3</sup>, M.W. Slater<sup>2</sup>, S.A. Wotton

*Cavendish Laboratory, University of Cambridge, Cambridge, CB3 0HE, UK<sup>4</sup>*

R. Arcidiacono<sup>5</sup>, G. Bocquet, A. Ceccucci, D. Cundy<sup>6</sup>, N. Doble<sup>7</sup>, V. Falaleev, L. Gatignon, A. Gonidec, P. Grafström, W. Kubischta, I. Mikulec<sup>8</sup>, A. Norton<sup>9</sup>, B. Panzer-Steindel, P. Rubin<sup>10</sup>, H. Wahl<sup>9</sup>

*CERN, CH-1211 Genève 23, Switzerland*

E. Goudzovski<sup>2</sup>, P. Hristov<sup>3</sup>, V. Kekelidze, L. Litov, D. Madigozhin, N. Molokanova, Yu. Potrebenikov, S. Stoynev, A. Zinchenko

*Joint Institute for Nuclear Research, Dubna, Russian Federation*

E. Monnier<sup>11</sup>, E. Swallow, R. Winston<sup>12</sup>

*The Enrico Fermi Institute, The University of Chicago, Chicago, IL 60126, USA*

R. Sacco<sup>13</sup>, A. Walker

*Department of Physics and Astronomy, University of Edinburgh, JCMB King's Buildings, Mayfield Road, Edinburgh, EH9 3JZ, UK*

W. Baldini, A. Gianoli

*INFN Sezione di Ferrara, I-44100 Ferrara, Italy*

P. Dalpiaz, P.L. Frabetti<sup>14</sup>, M. Martini, F. Petrucci, M. Savrié, M. Scarpa

*Dipartimento di Fisica dell'Università and INFN Sezione di Ferrara, I-44100 Ferrara, Italy*

M. Calvetti, G. Collazuol<sup>15</sup>, E. Iacopini, G. Ruggiero<sup>15</sup>

*Dipartimento di Fisica dell'Università and INFN Sezione di Firenze, I-50125 Firenze, Italy*

A. Bizzeti<sup>16</sup>, M. Lenti, M. Veltri<sup>17</sup>

*INFN Sezione di Firenze, I-50125 Firenze, Italy*

M. Behler, K. Eppard, M. Eppard, A. Hirstius<sup>3</sup>, K. Kleinknecht, U. Koch, P. Marouelli, L. Masetti<sup>18</sup>, U. Moosbrugger, C. Morales Morales, A. Peters<sup>3</sup>, R. Wanke, A. Winhart

*Institut für Physik, Universität Mainz, D-55099 Mainz, Germany<sup>19</sup>*

A. Dabrowski<sup>3</sup>, T. Fonseca Martin<sup>3</sup>, M. Velasco

*Department of Physics and Astronomy, Northwestern University, Evanston, IL 60208-3112, USA*

P. Cenci, P. Lubrano, M. Pepe

INFN Sezione di Perugia, I-06100 Perugia, Italy

G. Anzivino, E. Imbergamo<sup>\*</sup>, G. Lamanna<sup>15</sup>, A. Michetti, A. Nappi, M.C. Petrucci, M. Piccini, M. Valdata

Dipartimento di Fisica dell'Università and INFN Sezione di Perugia, I-06100 Perugia, Italy

C. Cerri, R. Fantechi

INFN Sezione di Pisa, I-56100 Pisa, Italy

F. Costantini, L. Fiorini<sup>20</sup>, S. Giudici, G. Pierazzini, M. Sozzi

Dipartimento di Fisica, Università degli Studi di Pisa and INFN Sezione di Pisa, I-56100 Pisa, Italy

I. Mannelli

Scuola Normale Superiore and INFN Sezione di Pisa, I-56100 Pisa, Italy

C. Cheshkov, J.B. Cheze, M. De Beer, P. Debu, G. Gouge, G. Marel, E. Mazzucato, B. Peyaud, B. Vallage

DSM/DAPNIA - CEA Saclay, F-91191 Gif-sur-Yvette, France

M. Holder, A. Maier<sup>3</sup>, M. Ziolkowski

Fachbereich Physik, Universität Siegen, D-57068 Siegen, Germany<sup>21</sup>

C. Biino, N. Cartiglia, F. Marchetto, N. Pastrone

INFN Sezione di Torino, I-10125 Torino, Italy

M. Clemencic<sup>3</sup>, S. Goy Lopez<sup>3</sup>, E. Menichetti

Dipartimento di Fisica Sperimentale dell'Università and INFN Sezione di Torino, I-10125 Torino, Italy

W. Wislicki

Soltan Institute for Nuclear Studies, Laboratory for High Energy Physics, PL-00-681 Warsaw, Poland<sup>22</sup>

H. Dibon, M. Jeitler, M. Markytan, G. Neuhofer, L. Widhalm

Österreichische Akademie der Wissenschaften, Institut für Hochenergiephysik, A-1050 Wien, Austria<sup>23</sup>

## ARTICLE INFO

### Article history:

Received 8 June 2009

Received in revised form 9 September 2009

Accepted 19 October 2009

Available online 21 October 2009

Editor: L. Rolandi

## ABSTRACT

A total of 368 415  $\Xi^0 \rightarrow \Lambda\pi^0$  and 31 171  $\bar{\Xi}^0 \rightarrow \bar{\Lambda}\pi^0$  were selected from data recorded in the NA48/1 experiment during 2002 data taking. From this sample, the polarization of  $\Xi^0$  and  $\bar{\Xi}^0$  hyperons was measured to be  $P_{\Xi^0} = -0.102 \pm 0.012(\text{stat}) \pm 0.008(\text{syst})$  and  $P_{\bar{\Xi}^0} = -0.01 \pm 0.04(\text{stat}) \pm 0.008(\text{syst})$ . The dependence of  $P_{\Xi^0}$  on the  $\Xi^0$  transverse momentum with respect to the primary proton beam is also presented. With the same data sample, the ratio of  $\bar{\Xi}^0$  and  $\Xi^0$  fluxes in proton collisions at 400 GeV/c on a beryllium target was measured.

© 2009 Elsevier B.V. All rights reserved.

<sup>\*</sup> Corresponding author.

E-mail address: [ermann.imbergamo@pg.infn.it](mailto:ermann.imbergamo@pg.infn.it) (E. Imbergamo).

<sup>1</sup> Present address: Rutherford Appleton Laboratory, Chilton, Didcot, Oxon, OX11 0QX, UK.

<sup>2</sup> Present address: University of Birmingham, Edgbaston, Birmingham, B15 2TT, UK.

<sup>3</sup> Present address: CERN, CH-1211 Genève 23, Switzerland.

<sup>4</sup> Funded by the UK Particle Physics and Astronomy Research Council.

<sup>5</sup> Present address: Dipartimento di Fisica Sperimentale dell'Università and INFN Sezione di Torino, I-10125 Torino, Italy.

<sup>6</sup> Present address: Istituto di Cosmogeofisica del CNR di Torino, I-10133 Torino, Italy.

## 1. Introduction

A significant polarization of  $\Lambda$  hyperons produced inclusively in the reaction  $p + Be \rightarrow \Lambda X$  has been detected three decades ago [1], and confirmed by later experiments, where also other hyperons have been found to exhibit the same feature. Several theoretical models relate the emerging polarization of the produced hyperons with various aspects of hadron interaction dynamics [2], but to date a definitive explanation has not yet emerged. The origin of the hyperon polarization has been discussed in terms of highly polarized  $s$  quarks which, by mechanisms based on semi-classical arguments like the Lund string model [3], the Thomas precession [4] or inspired by QCD [5], acquire a large negative polarization in the fragmentation process, before recombining with the beam proton remnants. The sign of the polarization depends on the SU(6) spin-flavor structure of the hyperon. In addition all models predict no polarization for anti-hyperons. On the experimental side, a rather extensive set of data on hyperon polarization, produced in inclusive reactions, can be found in literature. The most relevant ones are reviewed in [6]. In addition, the results in [7] have also to be considered with respect to this Letter, both as the first measurement of  $\Xi^0$  polarization and for comparison with the measurement reported here. Observations show that, in fixed target experiments, the polarization of the outgoing hyperon is normal to the production plane, and depends weakly on the target material. However the polarization depends more evidently on the primary beam energy and on the component of the hyperon momentum transverse to the primary beam direction (Pt), see for example [8]. Although a large variety of data exist for the  $\Lambda$ , less data are available for other hyperons. The  $\Xi^0$  polarization has been studied only by experiments [7] and [9], where it has been measured in a kinematical range of Pt around 1 GeV/c. In this work we present the measurements of  $\Xi^0$  polarization in the range  $0.37 < Pt < 0.73$  GeV/c, together with a measurement of  $\bar{\Xi}^0$  polarization averaged in the same Pt range.

<sup>7</sup> Present address: Dipartimento di Fisica, Università degli Studi di Pisa and INFN Sezione di Pisa, I-56100 Pisa, Italy.

<sup>8</sup> On leave from Österreichische Akademie der Wissenschaften, Institut für Hochenergiephysik, A-1050 Wien, Austria.

<sup>9</sup> Present address: Dipartimento di Fisica dell'Università and INFN Sezione di Ferrara, I-44100 Ferrara, Italy.

<sup>10</sup> On leave from University of Richmond, Richmond, VA, 23173, USA; supported in part by the US NSF under award #0140230. Present address: Department of Physics and Astronomy, George Mason University, Fairfax, VA 22030A, USA.

<sup>11</sup> Present address: Centre de Physique des Particules de Marseille, IN2P3-CNRS, Université de la Méditerranée, Marseille, France.

<sup>12</sup> Also at University of California, Merced, USA.

<sup>13</sup> Present address: Department of Physics, Queen Mary University, London, E1 4NS, UK.

<sup>14</sup> Present address: Joint Institute for Nuclear Research, Dubna 141980, Russian Federation.

<sup>15</sup> Present address: Scuola Normale Superiore and INFN Pisa, I-56100 Pisa, Italy.

<sup>16</sup> Also Dipartimento di Fisica dell'Università di Modena e Reggio Emilia, I-41100 Modena, Italy.

<sup>17</sup> Istituto di Fisica, Università di Urbino, I-61029 Urbino, Italy.

<sup>18</sup> Present address: Physikalisches Institut, Universität Bonn, D-53115 Bonn, Germany.

<sup>19</sup> Funded by the German Federal Minister for Education and research under contract 7MZ18P(4)-TP2.

<sup>20</sup> Present address: Institut de Física d'Altes Energies, Facultat Ciències, Universitat Autònoma de Barcelona, E-08193 Bellaterra, Spain.

<sup>21</sup> Funded by the German Federal Minister for Research and Technology (BMBF) under contract 056S174.

<sup>22</sup> Supported by the Committee for Scientific Research grants 5P03B10120, SPUB-M/CERN/P03/DZ210/2000 and SPB/CERN/P03/DZ146/2002.

<sup>23</sup> Funded by the Austrian Ministry for Traffic and Research under the contract GZ 616.360/2-IV GZ 616.363/2-VIII, and by the Fonds für Wissenschaft und Forschung FWF No. P08929-PHY.

From the same data set we have also determined the  $\Xi^0$  and  $\bar{\Xi}^0$  fluxes and their ratio as function of the energy.

## 2. The experimental setup

The NA48 experiment was originally designed for the measurement of direct CP violation in the decay of  $K_S^0$  and  $K_L^0$  mesons to two pions [10]. For this purpose, two beams providing respectively  $K_S^0$  and  $K_L^0$  decays were generated on two different targets by interaction of the same primary proton beam. The details of the NA48 design are extensively described in [10] or [11]. During the hyperon data taking in 2002 the  $K_L^0$  beam was switched off, and the intensity of  $K_S^0$  ( $\Xi^0$ ) beam was increased by a factor of about 100 with respect to the original NA48 data taking, with the necessary changes to the trigger system applied.

In brief, the setup was as follows: the protons were provided by the CERN SPS, accelerated up to 400 GeV/c momentum, then extracted in a 4.8 s spill every 16.8 s with an intensity of about  $5 \times 10^{10}$  protons per spill and transported to the target. The target was a beryllium cylinder of 0.2 cm diameter and 40 cm length. It was followed by a platinum absorber 24 mm thick in order to reduce the number of photons in the outgoing beam, and then by a sweeping magnet in which the protons non-interacting in the target were absorbed, in addition to charged particles generated in the proton interactions with the beryllium. A beam collimator defined a beam of neutral particles with a divergence of  $\pm 0.375$  mrad traveling at an angle of 4.2 mrad with respect to the proton beam direction and pointing to the center of the electromagnetic calorimeter about 120 m downstream. The decay region starts 6.2 m downstream of the target. It was contained in an evacuated (less than  $10^{-7}$  bar pressure) 89 m long and 2.4 m diameter steel tank, closed by a 0.3% radiation length thick polyamide (Kevlar) composite window.

The main NA48/1 detector elements were a magnetic spectrometer and a liquid-krypton electromagnetic calorimeter. The spectrometer was composed of two drift chambers upstream and two downstream of a dipole magnet. The magnetic field was directed vertically and produced a 265 MeV/c transverse momentum kick. The chambers provided 100  $\mu\text{m}$  spatial resolution on the track coordinates, resulting in a total momentum resolution of  $\sigma_p/p(\%) = 0.48 \oplus 0.015p$  (GeV/c). The liquid-krypton calorimeter (LKr) measured the energies, positions, and times of electromagnetic showers initiated by photons and electrons. The calorimeter had a structure of 13 212 square read-out cells of  $2 \times 2$  cm<sup>2</sup> cross-section and 127 cm length (27 radiation lengths) each. The cross section of the active volume had an octagonal shape of 240 cm inscribed diameter. The read-out cells were formed by longitudinally stretched copper-beryllium ribbons which acted as electrodes. The energy resolution of the calorimeter was  $\sigma(E)/E = 3.2\%/\sqrt{E_{[\text{GeV}]}} \oplus 9\%/E_{[\text{GeV}]} \oplus 0.42\%$  and the time resolution is better than 300 ps for photon energies above 20 GeV. Further detector elements were used in the trigger decision for the present measurement: a steel scintillator sandwich calorimeter with a length of 6.7 nuclear interaction lengths followed the liquid-krypton calorimeter, and measured energies and horizontal and vertical positions of hadron showers; a hodoscope, composed of 64 horizontal and 64 vertical scintillator strips, located about 1.6 m upstream of the LKr calorimeter; a scintillator-iron photon veto, made of seven rings placed in the decay region, covering an angular region starting at  $\sim 10$  mrad with respect to the beam axis.

A minimum bias trigger has been used for this measurement, based on information from the detector elements described above. A positive trigger decision required at least one coincidence between a vertical and a horizontal hodoscope scintillator strip, a two track signature in the drift chambers, the sum of the ener-

gies deposited in the electromagnetic and the hadron calorimeter larger than 30 GeV, and no photons escaping the decay region at large angle.

### 3. The strategy of the measurement

The  $\Xi^0$ s produced at the target proceed along the beam line and a large fraction of them decay within the fiducial decay region, mostly as  $\Xi^0 \rightarrow \Lambda\pi^0$ . Such decays can be exploited for the measurement of the  $\Xi^0$  polarization.

Due to parity violation, the decay is not symmetrical around the beam axis and the  $\Lambda$  is emitted preferentially along the direction of  $\Xi^0$  polarization.

The angular distribution of the  $\Lambda$  in the  $\Xi^0$  rest frame is described by:

$$\frac{dN}{N_0 d \cos \theta_{(\hat{n}_\Lambda, \vec{P}_{\Xi^0})}} \propto 1 + \alpha_{\Xi^0 \rightarrow \Lambda\pi^0} \hat{n}_\Lambda \cdot \vec{P}_{\Xi^0} \quad (1)$$

where  $\alpha(\Xi^0 \rightarrow \Lambda\pi^0)$  is the asymmetry parameter of the decay mode,  $\vec{P}_{\Xi^0}$  is the polarization of  $\Xi^0$  and  $\hat{n}_\Lambda$  is the direction of emission of the  $\Lambda$ .

It is clear from Eq. (1) that, in the case of  $\vec{P}_{\Xi^0} \neq 0$ , the distribution of the direction of emission of the  $\Lambda$  deviates from spherical symmetry and there is an enhancement of decays with the  $\Lambda$  pointing in the  $\vec{P}_{\Xi^0}$  direction. After a transformation into the laboratory rest frame, the distribution of the direction of emission of the  $\Lambda$  deviates from cylindrical symmetry (with the beam line as the axis of symmetry) and shows an enhancement of decays where the  $\Lambda$  is pointing into the direction of the  $\Xi^0$  polarization.

Although the modulus of  $\vec{P}_{\Xi^0}$  is unknown, its direction is known to be:

$$\vec{k} = \frac{\vec{p}_{\text{beam}} \times \vec{p}_{\Xi^0}}{|\vec{p}_{\text{beam}} \times \vec{p}_{\Xi^0}|} \quad (2)$$

where  $\vec{p}_{\text{beam}}$  is the momentum of the proton beam and  $\vec{p}_{\Xi^0}$  is the momentum of the  $\Xi^0$  in the laboratory reference system.

Note that no polarisation is expected unless the production angle is non-zero (4.2 mrad in our case). Indeed previous experiments, e.g. [1] and [9], have demonstrated that the polarisation vanishes when the production angle is zero. An excess of  $\Lambda$ 's along  $\hat{k}$  would indicate a non-zero polarization of the  $\Xi^0$ . Any excess may be quantified by measuring the mean value of the  $\Lambda$  coordinate along  $\hat{k}$  at any plane perpendicular to the beam line. In the standard NA48/1 coordinate system, the  $\hat{k}$  direction corresponds to the  $\hat{X}$  direction and any drift chamber is perpendicular to the beam line, e.g. the first one, herein called DCH1. Therefore it turns out that the distribution of the X coordinate of the  $\Lambda$  at DCH1 is sensitive to the  $\Xi^0$  polarization. Although it is the decay products of the mode  $\Lambda \rightarrow p\pi^-$  that are detected, at the energies of NA48/1 the proton travels very close to the  $\Lambda$  direction of flight, and so the X-coordinate distribution of the proton at DCH1 is still sensitive to  $\vec{P}_{\Xi^0}$ . Hence,  $\vec{P}_{\Xi^0}$  can be extracted by comparing the X coordinate distribution of the proton at DCH1 for real data with the distributions expected by Monte Carlo samples generated with different preset values of  $\vec{P}_{\Xi^0}$ . In the rest of the Letter, the  $\Xi^0$  polarization will simply be indicated as  $P_{\Xi^0}$  (instead of  $\vec{P}_{\Xi^0}$ ), meaning its non-null component along the X axis, whereas other components are assumed to be zero.

### 4. The event selection

A sample of  $\Xi^0 \rightarrow \Lambda\pi^0$  was selected for this measurement, with  $\Lambda \rightarrow p\pi^-$  and  $\pi^0 \rightarrow \gamma\gamma$ . A pair of positive and negative

tracks in the magnetic spectrometer, together with two electromagnetic clusters in the fiducial volume of the electromagnetic calorimeter are required. The clusters are requested to be spatially uncorrelated with respect to the two tracks ( $\text{Dist}_{\gamma, \text{track}} > 18$  cm) and in time with the two tracks within  $|T_\gamma - T_{\text{track}}| < 5$  ns. An energy dependent cut on the cluster width is applied. In addition, the two tracks are checked to be in time with each other ( $T_{\text{track}1} - T_{\text{track}2} < 5$  ns), to have a Closest Distance of Approach compatible with a common spatial origin ( $\text{CDA} < 2.2$  cm), and to have momenta kinematically compatible with a proton and a pion from a  $\Lambda$  decay ( $p_{\text{positive track}}/p_{\text{negative track}} > 3.5$ ). The invariant mass is required to be within  $3\sigma$  of the  $\Lambda$  mass, i.e.  $|M_{p,\pi^+} - M_{\Lambda}^{\text{PDG}}| < 0.0027$  GeV.

The two photons coordinates and energies are used together with tracks to calculate the quantity  $\vec{r}_{\text{cog}}$ , both to discard background events with unbalanced momentum ( $r_{\text{cog}} < 5$  cm) and to define the  $\Xi^0$  decay vertex. The quantity  $\vec{r}_{\text{cog}}$  is defined as:

$$\vec{r}_{\text{cog}} = \frac{\sum_i \vec{r}_i E_i}{\sum_i E_i}$$

where the sums run over tracks and photons. The  $\vec{r}_i$  are either the cluster positions of photons or coordinates of tracks extrapolated from before the spectrometer to the LKR calorimeter. The  $E_i$  are either photon cluster energies or are derived from the track momenta using the nominal particle masses. The target position and the energy center of gravity  $\vec{r}_{\text{cog}}$  define the line of flight of the  $\Xi^0$ . The  $\Xi^0$  decay vertex is defined as the point of closest approach between the  $\Xi^0$  line of flight and the  $\Lambda$  line of flight, determined by the known  $\Lambda$  decay vertex and momentum.

The closest distance of approach between the two specified lines is required to be compatible with a common spatial origin ( $\text{CDA} < 2.2$  cm), and the longitudinal z coordinate of the  $\Xi^0$  vertex is required to lie between the end of the beam collimator and  $5 \gamma_{\Xi^0} c \tau_{\Xi^0}$ , where  $\tau_{\Xi^0}$  is the  $\Xi^0$  lifetime and  $\gamma_{\Xi^0}$  is the average Lorentz factor of the  $\Xi^0$ s at NA48/1 energies ( $500 < \gamma_{\Xi^0} < 4000$  cm).

The  $\Xi^0$  decay vertex is also used to estimate the two photons invariant mass, required to be consistent with the  $\pi^0$  mass ( $0.12 < M_{\gamma\gamma} < 0.15$  GeV) and to determine the line of flight of the  $\pi^0$  as the line connecting the  $\Xi^0$  decay vertex with the centre of energy of the two photons.

In conclusion all the kinematic quantities of the event (decay vertices and four-momenta) are known and it is possible to check the invariant mass of the event. The final criteria of the event selection is that the  $\Lambda\pi^0$  invariant mass should be consistent with the nominal  $\Xi^0$  mass within 4 standard deviations, i.e.  $|M_{\Lambda\pi^0} - M_{\Xi^0}^{\text{PDG}}| < 0.021$  GeV.

In comparing these data with the Monte Carlo simulations, it has been observed that the drift chambers inefficiencies in detecting tracks close to the chambers inner edges are not correctly reproduced. An additional cut has therefore been applied, requiring the distance  $R_{\text{DCH1}}$  of the impact point of tracks at the first chamber from the chamber center to be  $R_{\text{DCH1}} > 13$  cm. The same cuts have been applied to select  $\bar{\Xi}^0$  events, obviously reversing the role of charges.

This selection leads to a very clean sample of  $368415 \Xi^0 \rightarrow \Lambda\pi^0$  events as shown in Fig. 1. The tail on left side is due to non-Gaussian effects in the resolution, well reproduced by the simulations, whereas the right tail is due to background events containing an in-time accidental gamma. Such background is small (less than 0.01%) and is neglected in the rest of the analysis.

For the extraction of the  $\bar{\Xi}^0$  polarization, a sample of 31171 events has been selected, also with a negligible contamination of background as shown in Fig. 1.

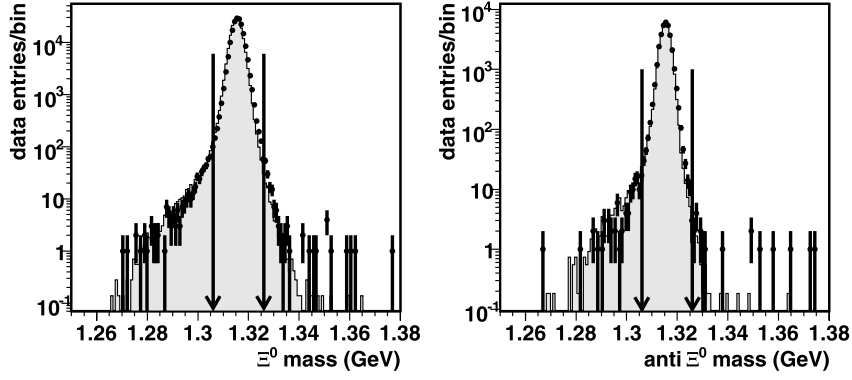


Fig. 1. The reconstructed masses for real data  $\Xi^0 \rightarrow \Lambda\pi^0$  (on the left) and  $\bar{\Xi}^0 \rightarrow \bar{\Lambda}\pi^0$  (on the right), and for MC data (in filled style). The arrows show the mass intervals for the selected events.

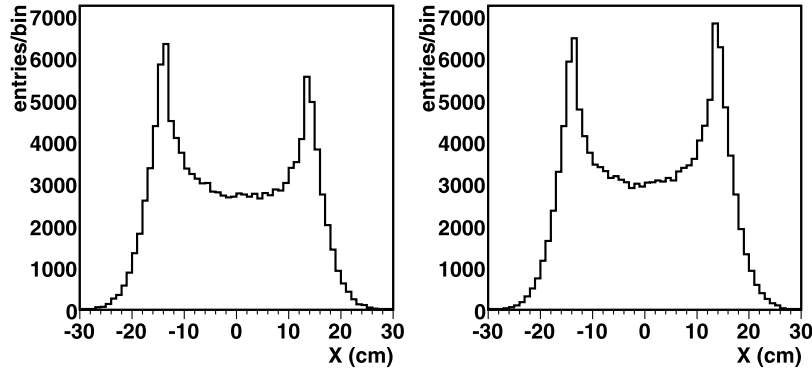


Fig. 2. X coordinate of proton at DCH1 for data with positive (on the left) and negative (on the right) magnet polarity.

## 5. Data analysis

For reasons independent of the present analysis, during 2002 data taking the polarity of the spectrometer magnet was switched regularly from positive to negative and vice versa. Since the acceptance of the detector in the two cases is different, the selected sample of  $\Xi^0 \rightarrow \Lambda\pi^0$  has been divided into two subsets, one with positive polarity of the spectrometer magnet and the other one with negative polarity of the magnet and two corresponding measurements of the polarization have been performed. The measurements are made by comparing the distribution of the X coordinate of the secondary proton at DCH1 for real data, see Fig. 2, with the corresponding distribution for polarized MC data.

The probability  $r$  of having a negative X coordinate for the proton hit is a very sensitive variable for estimating the  $\Xi^0$  polarization: Fig. 3 shows the  $r$  probability for data (the horizontal line), and for the MC samples (the circles) generated with a preset values of the  $\Xi^0$  polarization, indicated on the abscissa.

Although the actual value of  $P_{\Xi^0}$  could simply be extracted from the plot, a maximum likelihood method is performed in order to obtain a more accurate estimate of the polarization. Assuming that there is a linear dependence of  $r$  with respect to the  $\Xi^0$  polarization and binomial distributed number of events with  $x < 0$ ,  $P_{\Xi^0}$  can be extracted by maximizing the log-likelihood<sup>24</sup>:

<sup>24</sup> For each given sample  $j$  of data, we assume that  $n_j^-$  is binomial distributed, with a probability  $r_j$  of having an event with  $x < 0$  linearly dependent on the  $\Xi^0$  polarization, e.g.  $r_j = r_0 + aP_j$ . Therefore, the probability  $r_j$  of observing  $n_j^-$  events for the  $j$ -th sample of data is:

$$P(n_j^-) = \binom{N_j}{n_j^-} r_j^{n_j^-} (1-r_j)^{N_j-n_j^-} = \binom{N_j}{n_j^-} r_j^{n_j^-} (1-r_j)^{n_j^+}$$

$$\begin{aligned} \ln L = & n_{\text{data}}^- \ln(r_{\text{data}}) + n_{\text{data}}^+ \ln(1-r_{\text{data}}) \\ & + \sum_{i=1}^{\text{mc samples}} n_{\text{mc}(i)}^- \ln(r_{\text{mc}(i)}) + n_{\text{mc}(i)}^+ \ln(1-r_{\text{mc}(i)}) \end{aligned} \quad (3)$$

For each event sample,  $n_-$  and  $n_+$  are the number of events with  $x < 0$  or  $x > 0$ , among the total amount  $N = n_- + n_+$  of the events;  $r_{\text{data}} = r_0 + aP_{\Xi^0}$  and  $r_{\text{mc}(i)} = r_0 + aP_{\text{mc}(i)}$  by hypothesis of linearity, and  $P_{\text{mc}(i)}$  are the known  $\Xi^0$  polarization of the Monte Carlo samples.  $P_{\Xi^0}$ ,  $r_0$  and  $a$  are free parameters to be determined by maximizing the  $\ln L$  function. Among them,  $P_{\Xi^0}$  is the parameter that we want to measure, whereas  $r_0$  and  $a$  are ancillary parameters introduced by the method.

The method returns the following values for the two subsets of data:

$$P_{\Xi^0} = -0.114 \pm 0.017(\text{stat}) \quad (\text{positive magnet polarity}) \quad (3a)$$

$$P_{\Xi^0} = -0.089 \pm 0.018(\text{stat}) \quad (\text{negative magnet polarity}) \quad (3b)$$

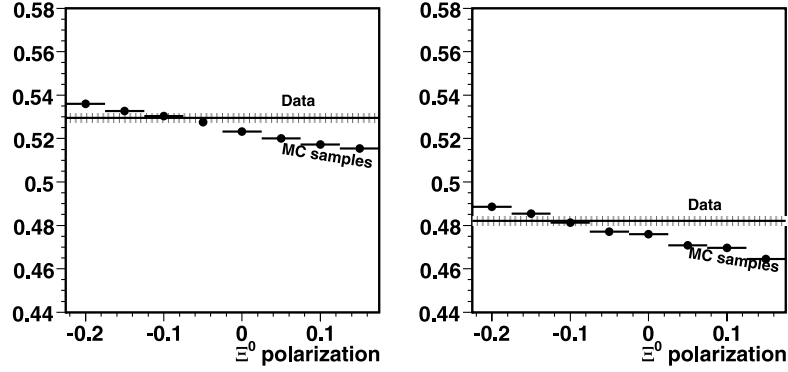
The two results are statistically compatible within 0.9 standard deviations. Fig. 4 shows a comparison between the X coordinate of proton at DCH1 for data and simulated MC data generated with  $\Xi^0$  polarization given by the two measurements (3a) and (3b).

Table 1 shows a summary of detailed systematic checks for the two subsets with positive polarity of the DCH magnet (mag+)

and the probability for the full set of observations is the likelihood function

$$L = \prod_{j=1}^{\text{all samples}} P(n_j^-) = P(n_{\text{data}}^-) \prod_{i=1}^{\text{mc samples}} P(n_{\text{mc}(i)}^-)$$

The formula (3) is the  $\ln L$ , where the irrelevant constant terms are omitted.



**Fig. 3.**  $r$  probability for data (the horizontal line), and for the MC samples (the circles) generated with a preset values of the  $\Xi^0$  polarization for data with positive (on the left) and negative (on the right) magnet polarity.

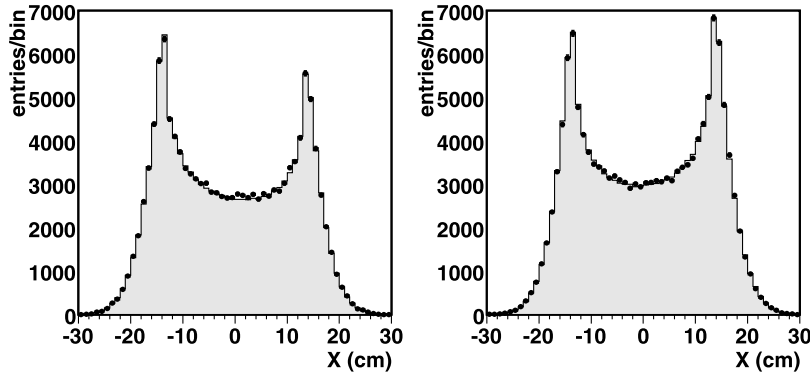


**Fig. 4.** Comparison between X coordinate of proton at DCH1 for data (the dots) and simulated MC data (in filled style) with positive (on the left) and negative (on the right) magnet polarity. The MC data have been generated with  $\Xi^0$  polarization given by the two measurements (3a) and (3b).

**Table 1**

Summary of the systematic contributions to the measurement.

| Systematic  | mag+  | mag-  |
|---|-------|-------|
| Beam modeling   | 0.007 | 0.003 |
| DCH1 inefficiencies at small radii                      | 0.005 | 0.002 |
| Likelihood hypothesis: quadratic dependence             | 0.001 | 0.003 |
| Uncertainty on $\alpha(\Xi^0 \rightarrow \Lambda\pi^0)$ | 0.004 | 0.005 |
| Uncertainty on $\alpha(\Lambda \rightarrow p\pi^-)$     | 0.002 | 0.002 |
| Subsample overall                                       | 0.009 | 0.007 |
| Subsample average                                       | 0.008 |       |

and negative polarity (mag-). In particular, the likelihood hypothesis has been checked by adding a quadratic dependence of the  $r$  variable on  $P_{\Xi^0}$ . The difference between the new extrapolated value of  $P_{\Xi^0}$  and the previous one has been taken as an estimate of the systematic error. The effect of non-exact values for the  $\alpha(\Xi^0 \rightarrow \Lambda\pi^0)$  and  $\alpha(\Lambda \rightarrow p\pi^-)$  parameters used in the generation of Monte Carlo samples has been checked by varying them (one at time) by  $\pm 1\sigma$  around their nominal PDG value. Half of the difference between the two new values obtained for  $P_{\Xi^0}$  has been taken as systematic error. The systematic uncertainty due to the inaccuracy in reproducing the drift chambers efficiencies at small radii has also been studied. The dependence of  $P_{\Xi^0}$  on the DCH1 inner radius cut vanishes around the nominal cut value (for both magnet polarities). The difference between the measured polarization at the standard cut and the plateau value of the  $P_{\Xi^0}$  versus RDCH1 distribution is taken as systematic error. In a similar way, the effect of inaccuracies in the  $\Xi^0$  beam modeling in the Monte Carlo has been studied by varying the cut on COG, which is sen-

sitive to the beam shape. Combining the measurement on the two subsets, the overall result is:

$$P_{\Xi^0} = -0.102 \pm 0.012(\text{stat}) \pm 0.008(\text{syst})$$

The polarization of  $\Xi^0$ s has also been measured as a function of the transverse momentum  $P_t$ , dividing the data into  $P_t$  intervals and performing the analysis separately on each interval. Fig. 5 shows the value of the  $\Xi^0$  polarization for different bins of  $P_t$  (black circles), compared to the previous measurements. The values in each  $P_t$  interval are listed in Table 2.

Finally, the  $\bar{\Xi}^0$  polarization has been estimated, for the two subsets of data with different magnet polarity, as:

$$P_{\bar{\Xi}^0} = -0.06 \pm 0.06(\text{stat}) \quad (\text{positive magnet polarity})$$

$$P_{\bar{\Xi}^0} = +0.03 \pm 0.05(\text{stat}) \quad (\text{negative magnet polarity})$$

The two values are consistent with each other, and their average is:

$$P_{\bar{\Xi}^0} = -0.01 \pm 0.04(\text{stat}) \pm 0.008(\text{syst})$$

The  $\bar{\Xi}^0$  polarization is consistent with zero, although with a large statistical error. The same systematic error as  $P_{\Xi^0}$  has been associated to the measurement because no new effects are involved in the  $\bar{\Xi}^0$  analysis.

## 6. Measurement of the $\bar{\Xi}^0/\Xi^0$ flux ratio

The same data sample of  $\Lambda\pi^0$  and  $\bar{\Lambda}\pi^0$  decays used for the  $\Xi^0$  polarization measurement was also exploited to determine the production ratio between  $\bar{\Xi}^0$  and  $\Xi^0$  hyperons at the target, using the same selection criteria.

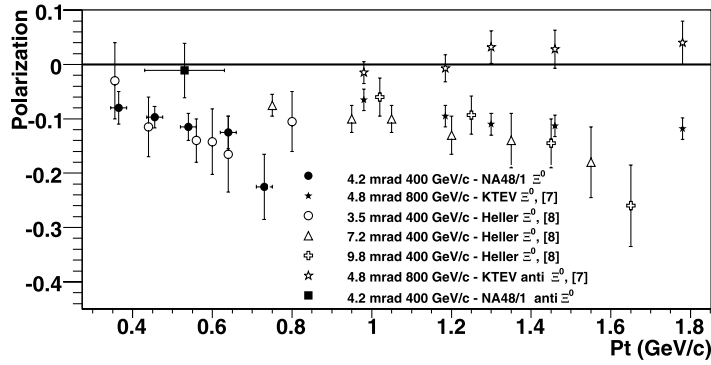


Fig. 5. NA48/1 and previous measurements of  $\Xi^0$  and  $\bar{\Xi}^0$  polarization as function of the transverse momentum Pt.

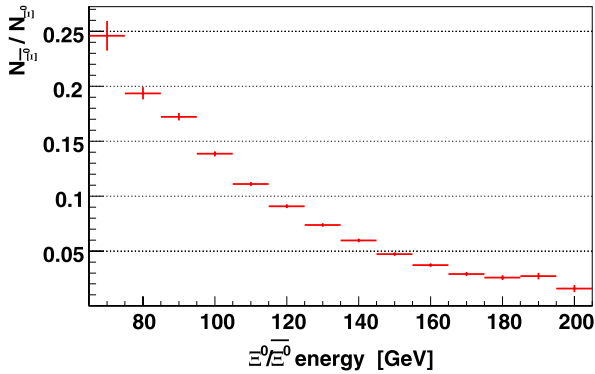


Fig. 6. Measurement of the  $\bar{\Xi}^0$  to  $\Xi^0$  flux ratio as function of energy.

Table 2

Tabulated values NA48/1 measured values of the  $\Xi^0$  polarization as function of the transverse momentum Pt.

| Pt (GeV/c)      | Polarization     |
|-----------------|------------------|
| $0.36 \pm 0.02$ | $-0.08 \pm 0.03$ |
| $0.46 \pm 0.02$ | $-0.10 \pm 0.02$ |
| $0.54 \pm 0.02$ | $-0.12 \pm 0.02$ |
| $0.64 \pm 0.02$ | $-0.13 \pm 0.03$ |
| $0.73 \pm 0.02$ | $-0.22 \pm 0.06$ |

Table 3

Tabulated values of the  $\bar{\Xi}^0$  to  $\Xi^0$  flux ratio as function of energy.

| Energy interval | $\bar{\Xi}^0/\Xi^0$ flux ratio | Energy interval | $\bar{\Xi}^0/\Xi^0$ flux ratio |
|-----------------|--------------------------------|-----------------|--------------------------------|
| 65–75 GeV       | $0.246 \pm 0.014$              | 135–145 GeV     | $0.060 \pm 0.002$              |
| 75–85 GeV       | $0.194 \pm 0.006$              | 145–155 GeV     | $0.047 \pm 0.002$              |
| 85–95 GeV       | $0.172 \pm 0.003$              | 155–165 GeV     | $0.037 \pm 0.002$              |
| 95–105 GeV      | $0.139 \pm 0.002$              | 165–175 GeV     | $0.029 \pm 0.002$              |
| 105–115 GeV     | $0.111 \pm 0.002$              | 175–185 GeV     | $0.026 \pm 0.002$              |
| 115–125 GeV     | $0.091 \pm 0.002$              | 185–195 GeV     | $0.027 \pm 0.003$              |
| 125–135 GeV     | $0.074 \pm 0.002$              | 195–205 GeV     | $0.016 \pm 0.003$              |

Fig. 6 shows the  $\bar{\Xi}^0$  to  $\Xi^0$  flux ratio as a function of energy. It falls with energy, as expected. The values in each energy bin are listed in Table 3.

## 7. Conclusion

In conclusion we confirm and improve the only existing measurement [9] of  $\Xi^0$  polarization created with transverse Pt momentum less than 1 GeV/c. We also confirm the previous result [7] of zero polarization of the  $\bar{\Xi}^0$  in the same kinematical region.

## Acknowledgements

It is a pleasure to thank the technical staff of the participating laboratories, universities and affiliated computing centers for their efforts in the construction of the NA48/1 apparatus, in the operation of the experiment, and in the processing of the data.

## References

- [1] G. Bunce, et al., Phys. Rev. Lett. 36 (1976) 1113.
- [2] J. Felix, Mod. Phys. Lett. A 14 (1999) 827.
- [3] B. Andersson, et al., Phys. Lett. B 85 (1979) 417.
- [4] T.A. Degrand, H.I. Miettinen, Phys. Rev. D 23 (1981) 1227; T.A. Degrand, H.I. Miettinen, Phys. Rev. D 24 (1981) 2419; T.A. Degrand, H.I. Miettinen, Phys. Rev. D 31 (1985) 661 (Erratum).
- [5] G.W. Dharmaratna, G.R. Goldstein, Phys. Rev. D 41 (1990) 1731; J. Szwed, Phys. Lett. B 105 (1981) 403.
- [6] A. Bravar, in: SPIN 98 Proceedings of the 13th International Symposium on High Energy Physics, Protvino, Russia, 8–12 September 1998.
- [7] E. Abouzaid, et al., KTeV Collaboration, Phys. Rev. D 75 (2007) 012005.
- [8] B. Lundberg, et al., Phys. Rev. D 40 (1989) 3557.
- [9] K. Heller, et al., Phys. Rev. Lett. 51 (1983) 22.
- [10] V. Fanti, et al., NA48 Collaboration, Nucl. Instrum. Methods A 574 (2007) 433.
- [11] J.R. Batley, et al., NA48 Collaboration, Phys. Lett. B 544 (2002) 97.